

# Hybrid functional study on structural and electronic properties of oxides

Sohee Park, Bora Lee, Sang Ho Jeon, Seungwu Han\*

Department of Materials Science and Engineering, Seoul National University, Seoul 151-744, Republic of Korea

## ARTICLE INFO

### Article history:

Received 10 July 2010

Accepted 7 September 2010

Available online 17 September 2010

### Keywords:

Hybrid functional

HSE06

Energy gap

Lattice parameters

Band offset

## ABSTRACT

The hybrid functional method within the HSE06 scheme is tested on various oxides such as TiO<sub>2</sub>, SrTiO<sub>3</sub>, ZnO, SnO<sub>2</sub>, MgO, SiO<sub>2</sub>, and Al<sub>2</sub>O<sub>3</sub>. Since the canonical mixing parameter still underestimates the energy gap, we optimize it by fitting the energy gap to the experimental value. It is found that optimized values lie between 0.2 and 0.4 depending on the material. The structural properties are examined and the lattice parameters calculated with the HSE06 functional are in better agreement with experiment compared to (semi)local functional results. The relative shifts in the valence and conduction edges are provided, which can serve as first-order corrections to the semilocal functional results on defect levels or interfacial band offsets.

© 2010 Elsevier B.V. All rights reserved.

## 1. Introduction

First-principles methods based on conventional density functional theory (DFT) such as the local density approximation (LDA) or the generalized gradient approximation (GGA) have been successfully applied to studying various properties in a wide range of materials. To be specific, structural parameters and atomic positions agree with experimental values typically within 3% and mechanical properties such as elastic constants are reproduced within 5% errors in most cases. This level of accuracy is particularly impressive given that exchange–correlation energies of electrons are greatly simplified in (semi)local functionals. However, one critical drawback in (semi)local functionals is that the energy gap is severely underestimated by 30–40%. This is because DFT is based on the ground-state formalism and the energy gap is essentially an excited-state property. The energy-gap underestimation in the conventional DFT limits its application in several places. For example, the position of defect levels with respect to band edges inevitably suffer from the error in the band-gap. In addition, Schottky barriers formed at metal–insulator interfaces are also underestimated.[1]

To overcome the band-gap problem in (semi)local functionals, several methods beyond LDA or GGA have been attempted. Among them, the GW method is the seamless extension of DFT but the method is too expensive to be used in complex systems.[2] Recently, hybrid functional methods are receiving increasing

attention. In these methods, the energy gap is increased by replacing a part, typically one quarter, of GGA functionals with the Hartree–Fock (HF) style exact exchange energy formulated as follows:

$$E_x^{\text{HF}} = -\frac{e^2}{2} \sum_{ij} \iint d^3r d^3r' \frac{\phi_i^*(r)\phi_j^*(r')\phi_i(r')\phi_j(r)}{|r-r'|}, \quad (1)$$

where  $\phi_i$ 's are the occupied wave functions and  $i$  represents a quantum-number set comprising band and  $k$ -point indexes. Even though the energy gaps from hybrid functional methods are usually in good agreement with experiment, the sheer computational cost has prohibited a wide use of the method.

Several forms of the hybrid method have been proposed to date and they differ on how the exact exchange energy is mixed in the energy functional. Recently, the one proposed by Heyd–Scuseria–Ernzerhof [3] has been found to give satisfactory results on various solid state systems.[4] In this method, a screened Coulomb potential is used in the HF energy. This is accomplished by splitting the Coulomb operator into short-range (SR) and long-range (LR) parts:

$$\frac{1}{r} = S_\mu(r) + L_\mu(r) = \frac{\text{erfc}(\mu r)}{r} + \frac{\text{erf}(\mu r)}{r}. \quad (2)$$

Then, the HF exchange energy in Eq. (1) is calculated by making use of  $S_\mu(r)$ . The resulting exchange–correlation functional is given as follows:

$$E_{xc}^{\text{HSE}} = \alpha E_x^{\text{HF,SR}}(\mu) + (1 - \alpha) E_x^{\text{PBE,SR}}(\mu) + E_x^{\text{PBE,LR}}(\mu) + E_c^{\text{PBE}}, \quad (3)$$

\* Corresponding author.

E-mail address: [hansw@snu.ac.kr](mailto:hansw@snu.ac.kr) (S. Han).

**Table 1**

Computational parameters used in the calculations. The cutoff energy ( $E_{\text{cut}}$ ) and  $k$ -point meshes sampled in the first Brillouin zone.

	$E_{\text{cut}}$ (eV)	$k$ -point mesh
Si	300	$4 \times 4 \times 4$
GaAs	250	$4 \times 4 \times 4$
TiO <sub>2</sub> (rutile)	500	$4 \times 4 \times 6$
SrTiO <sub>3</sub>	500	$4 \times 4 \times 4$
ZnO	500	$5 \times 5 \times 3$
SnO <sub>2</sub>	550	$3 \times 3 \times 5$
Diamond	450	$6 \times 6 \times 6$
MgO	500	$5 \times 5 \times 5$
SiO <sub>2</sub>	450	$3 \times 3 \times 3$
Al <sub>2</sub> O <sub>3</sub> (corundum)	500	$4 \times 4 \times 4$

where  $E_c^{\text{PBE}}$  is the PBE functional for the correlation energy [5]. In Eq. (3), the PBE exchange energy functionals are modified in accordance with the screened Coulomb potential but still depends on the electronic density and its gradient only.[3] The mixing coefficient  $\alpha$  in Eq. (3) is set to 1/4 which is supported by a perturbation theory [6] but one can use it as a variable to fit the energy gap. For the screening parameter  $\mu$ , 0.2–0.3 Å<sup>-1</sup> is typically used and we choose 0.2 Å<sup>-1</sup> in the present work (so called HSE06).

Even though the hybrid functional method provides a promising solution to remedy the energy-gap problem, it has not been tested thoroughly against various kinds of materials. In the present work, we apply the hybrid method on representative oxide materials and examine closely how electronic and structural properties change from the LDA or GGA results.

## 2. Computational methods and model systems

Throughout this work, we use Vienna *Ab-initio* Simulation Package (VASP).[7] The electron–ion interactions are modeled by the projector-augmented wave (PAW) pseudopotential.[8] The energy cutoffs and  $k$ -point meshes are chosen on the basis of convergence in the total energy and stress tensor within 5 meV/atom and 5 kbar, respectively. The selected parameter sets are enlisted in Table 1. For model systems, we choose TiO<sub>2</sub> (rutile), SrTiO<sub>3</sub> (cubic), ZnO (wurtzite), SnO<sub>2</sub> (rutile), MgO (rocksalt), SiO<sub>2</sub> ( $\alpha$ -quartz), and Al<sub>2</sub>O<sub>3</sub> (corundum), in the order of increasing energy gaps. The energy gap and structural properties are experimentally well established for these representative oxides. For comparison, we also calculate on diamond and semiconductors such as Si and GaAs. The atomic positions and lattice parameters are relaxed until atomic forces and stress tensors are reduced to within 0.02 eV/Å and 5 kbar, respectively.

## 3. Results

### 3.1. Band-gap

First, we calculate the fundamental energy gaps of various oxides using HSE06 functional and mark them as filled circles in Fig. 1(a). For comparison, GGA and LDA results are also presented in squares and triangles, respectively. The  $x$  coordinate of each point corresponds to an experimental data [9–16] while  $y$  coordinate represents the theoretical results. It is seen that the results from (semi)local functionals are smaller than experimental values by 30–40%. The biggest reduction is identified for ZnO where the LDA or GGA energy gaps are only  $\sim$ 25% of the reference value. In contrast, the HSE06 functional with  $\alpha = 0.25$  significantly increases the energy gap and the discrepancy with experiment is less than 10% on average. (The largest error is found for ZnO.) It is also noted that energy gaps of the non-oxide materials are in better agreement with experiment compared to oxides.

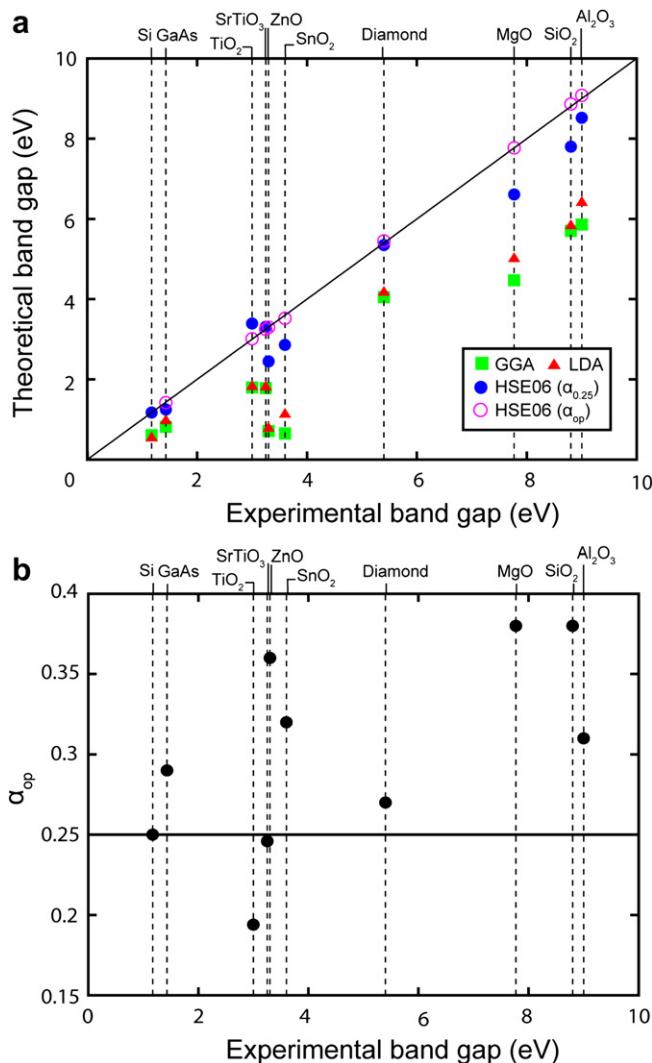


**Fig. 1.** (a) The energy gaps of various materials are compared between experiment ( $x$  coordinate) and theory ( $y$  coordinate). The experimental data are quoted from following references: Si [9], diamond [9], GaAs [9], TiO<sub>2</sub> [10], SrTiO<sub>3</sub> [11], ZnO [12], SnO<sub>2</sub> [13], MgO [14], SiO<sub>2</sub> [15], Al<sub>2</sub>O<sub>3</sub> [16]. (b) The optimized mixing coefficient ( $\alpha_{op}$ ) obtained by fitting the energy gap to the experimental data.

Even though computational results with the canonical value of  $\alpha$  are more satisfactory than LDA or GGA results, the energy gap is consistently underestimated for most oxides. To reduce the discrepancy with experiment, we try to adjust  $\alpha$  by manually increasing or decreasing the value. The crystal structures are re-optimized whenever  $\alpha$  is changed. In Fig. 1(a), the fitted energy gaps are displayed as empty circles and the optimized mixing coefficient  $\alpha_{op}$ 's are plotted in Fig. 1(b). It is noted that most  $\alpha_{op}$ 's are bigger than 0.25. This is because the energy gap is underestimated in the standard HSE06 scheme, which can be resolved by increasing the relative weight of the HF term. Note that the energy gap is overestimated in original HF calculations. For TiO<sub>2</sub> and SrTiO<sub>3</sub>, it is noticeable that  $\alpha_{op}$  is lowered slightly to 0.194 and 0.246, respectively.

### 3.2. Structural properties

Next, we examine structural properties represented by lattice parameters. The theoretical and experimental lattice parameters are compiled in Table 2. The deviation from the experimental value is provided in the parenthesis. To capture the general behavior, the average error for each material is plotted in Fig. 2. It is noticeable

**Table 2**

Theoretical and experimental lattice parameters in Å. The experimental data are quoted from following references: Si [9], diamond [9], GaAs [17], TiO<sub>2</sub> [18], SrTiO<sub>3</sub> [19], ZnO [20], SnO<sub>2</sub> [21], MgO [22], SiO<sub>2</sub> [23], and Al<sub>2</sub>O<sub>3</sub> [24].

	Exp.	LDA	GGA	HSE06 ( $\alpha_{0.25}$ )	HSE06 ( $\alpha_{op}$ )
Si	5.430	5.400 (−0.6%)	5.466 (0.7%)	5.430 (0.0%)	5.430 (0.0%)
GaAs	5.642	5.624 (−0.3%)	5.762 (2.1%)	5.695 (0.9%)	5.687 (0.8%)
TiO <sub>2</sub>	a: 4.593 c: 2.956	a: 4.558 (−0.8%) c: 2.926 (−1.0%)	a: 4.650 (1.2%) c: 2.972 (0.5%)	a: 4.588 (−0.1%) c: 2.951 (−0.2%)	a: 4.602 (0.2%) c: 2.954 (−0.1%)
SrTiO <sub>3</sub>	3.905	3.863 (−1.1%)	3.945 (1.0%)	3.900 (−0.1%)	3.907 (0.1%)
ZnO	a: 3.250 c: 5.210	a: 3.201 (−1.5%) c: 5.154 (−1.1%)	a: 3.297 (1.4%) c: 5.289 (1.5%)	a: 3.253 (0.1%) c: 5.260 (1.0%)	a: 3.242 (−0.2%) c: 5.239 (0.6%)
SnO <sub>2</sub>	a: 4.737 c: 3.185	a: 4.732 (−0.1%) c: 3.196 (0.3%)	a: 4.820 (1.8%) c: 3.240 (1.7%)	a: 4.756 (0.4%) c: 3.193 (0.3%)	a: 4.738 (0.0%) c: 3.183 (−0.1%)
Diamond	3.567	3.535 (−0.6%)	3.584 (0.8%)	3.545 (−0.3%)	3.544 (−0.3%)
MgO	4.190	4.157 (−0.8%)	4.242 (1.2%)	4.196 (0.1%)	4.171 (−0.5%)
SiO <sub>2</sub>	a: 4.915 c: 5.406	a: 4.888 (−0.5%) c: 5.388 (−0.3%)	a: 4.994 (1.6%) c: 5.489 (1.5%)	a: 4.930 (0.3%) c: 5.421 (0.3%)	a: 4.922 (0.1%) c: 5.409 (0.1%)
Al <sub>2</sub> O <sub>3</sub>	a: 4.759 c: 12.991	a: 4.730 (−0.6%) c: 12.912 (−0.6%)	a: 4.806 (1.0%) c: 13.119 (1.0%)	a: 4.755 (−0.1%) c: 12.979 (−0.1%)	a: 4.745 (−0.3%) c: 12.942 (−0.4%)

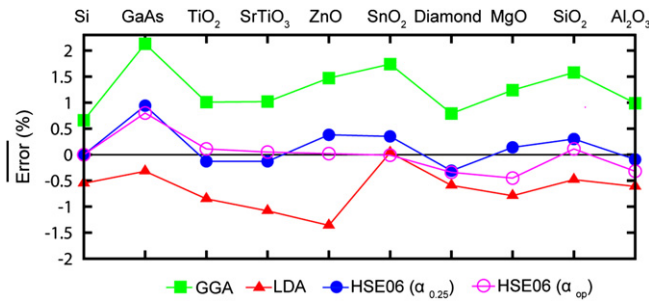


**Fig. 2.** The average errors in lattice parameters with respect to the experimental data. When the structure is not cubic, as in TiO<sub>2</sub>, ZnO, SnO<sub>2</sub>, SiO<sub>2</sub>, and Al<sub>2</sub>O<sub>3</sub>, the average error is calculated as  $[2 \times (\text{error in } a) + (\text{error in } c)]/3$ .

that LDA underestimates the lattice parameters while GGA overestimates them by similar amounts. Interestingly, the lattice parameters with hybrid functional lie in between LDA and GGA results and are in best agreement with experiment. This indicates that adding the HF exchange interactions effectively reduces the lattice parameters from GGA values. This would originate from the enhanced localization of electrons which favors tight interatomic bonding. In Fig. 2, it is also confirmed that optimizing  $\alpha$  does not affect the lattice parameters significantly although the lattice parameters are slightly reduced as  $\alpha_{op}$  is bigger than 0.25.

### 3.3. Shifts in band edges

Lastly, we investigate how the valence and conduction edges shift with respect to GGA results. To this end, it is necessary to set the common reference energy between GGA and HSE06 calculations. In the present work, we make use of electrostatic potentials

**Table 3**

Shifts in conduction band minimum (CBM) and valence band maximum (VBM) of HSE 06 results (with  $\alpha_{op}$ ) with respect to PBE values. The unit is eV.

	$\Delta\text{CBM}$	$\Delta\text{VBM}$
Si	0.38	−0.18
GaAs	0.51	−0.11
TiO <sub>2</sub>	0.72	−0.49
SrTiO <sub>3</sub>	0.67	−0.80
ZnO	1.09	−1.51
SnO <sub>2</sub>	1.66	−1.21
Diamond	1.10	−0.30
MgO	1.73	−1.57
SiO <sub>2</sub>	1.40	−1.76
Al <sub>2</sub> O <sub>3</sub>	1.97	−1.25

contributed by electrons and ions. (The ionic potentials are represented by PAW pseudopotentials.) When averaged over the unit cell, the reference energy is equal to zero because of the charge neutrality condition. We note that charge densities from HSE06 calculations are almost the same as those from the PBE functional, and this validates the use of electrostatic potentials in determining the common reference point. In Table 3, the shifts of conduction band minimum ( $\Delta\text{CBM}$ ) and valence band maximum ( $\Delta\text{VBM}$ ) are enlisted. Overall, valence and conduction edges in oxides shift by similar amounts in oxides. In contrast, the band-gap increases in non-oxide materials are mainly driven by up-shift of conduction bands.

The information provided in Table 3 would be useful in many places. First, it was shown in Ref. [25] that the position of a localized defect level is almost invariant between GGA and hybrid functional methods when it is aligned with the common reference energy. Therefore, the relative shifts in Table 3 can be used to correct defect levels calculated with GGA methods. Second, Table 3 can be also utilized in exploring band offsets in heterointerfaces formed between metals, oxides, and semiconductors. The full-blown hybrid functional study on heterointerfaces would be extremely time-consuming within most computational facilities at present. As an alternative approach, one can first perform a GGA calculation and extract band offsets from the potential line-up. Then, using the band shifts in Table 3, the gap-corrected offset values can be obtained. The underlying assumption here is that the interface dipole is well described within conventional DFT. As a specific example, if the interface is formed between a metal and an oxide, the correct valence band offset ( $E_{\text{VBO}}^{\text{corr}}$ ) is given as follows:

$$E_{\text{VBO}}^{\text{corr}} = E_{\text{VBO}}^{\text{PBE}} + \Delta\text{VBM}, \quad (4)$$

where  $E_{\text{VBO}}^{\text{PBE}}$  is the valence band offset from the PBE calculation and  $\Delta\text{VBM}$  is the shift in the valence band given in Table 3.

## 4. Conclusion

In summary, we carried out extensive calculations on various oxides such as TiO<sub>2</sub>, SrTiO<sub>3</sub>, ZnO, SnO<sub>2</sub>, MgO, SiO<sub>2</sub>, and Al<sub>2</sub>O<sub>3</sub> using the HSE06 functional. Since the canonical mixing parameter still underestimated the energy gap, we optimized it to fit the energy gap to the experimental value. The optimized values lie between 0.2 and 0.4 depending on the material. The structural properties are examined and the lattice parameters are in better agreement with experiment compared to (semi)local functional results. The relative

shifts in the valence and conduction edges were evaluated, which will serve as a first-order correction to the (semi)local functional results on defect levels or interfacial band offsets.

### Acknowledgements

This research was supported by Basic Science Research Program through the National Research Foundation of Korea (NRF) funded by the Ministry of Education, Science and Technology (2010-0011085). The authors would like to acknowledge the support from the KISTI Supercomputing Center (KSC-2009-S03-0008).

### References

- [1] S.H. Jeon, B.H. Park, J. Lee, B. Lee, S. Han, *Appl. Phys. Lett.* 89 (2006) 042904.
- [2] M. van Schilfgaarde, T. Kotani, S. Faleev, *Phys. Rev. Lett.* 96 (2006) 226402.
- [3] J. Heyd, G.E. Scuseria, M. Ernzerhof, *J. Chem. Phys.* 118 (2003) 8207–8215.
- [4] J. Paier, M. Marsman, K. Hummer, G. Kresse, I.C. Gerber, J.G. Ángyán, *J. Chem. Phys.* 124 (2006) 154709.
- [5] J.P. Perdew, K. Burke, M. Ernzerhof, *Phys. Rev. Lett.* 77 (1996) 3865–3868.
- [6] J.P. Perdew, M. Ernzerhof, K. Burke, *J. Chem. Phys.* 105 (1996) 9982–9985.
- [7] G. Kresse, J. Furthmüller, *Phys. Rev. B* 54 (1996) 11169–11186.
- [8] P.E. Blöchl, *Phys. Rev. B* 50 (1994) 17953–17979.
- [9] C. Kittel, *Introduction to Solid State Physics*, eighth ed. Wiley, New York, 2005.
- [10] J. Pascual, J. Camassel, H. Mathieu, *Phys. Rev. B* 18 (1978) 5606–5614.
- [11] K.V. Benthem, C. Elsasser, R.H. French, *J. Appl. Phys.* 90 (2001) 6156–6164.
- [12] V. Srikant, D.R. Clarke, *J. Appl. Phys.* 83 (1998) 5447–5451.
- [13] D. Fröhlich, R. Kenklies, *Phys. Rev. Lett.* 41 (1978) 1750–1751.
- [14] D.M. Roessler, W.C. Walker, *Phys. Rev.* 159 (1967) 733–738.
- [15] R.B. Laughlin, *Phys. Rev. B* 22 (1980) 3021–3029.
- [16] B.D. Evans, G.J. Pogatschnik, Y. Chen, *Nucl. Instr. Meth. Phys. Res. B* 91 (1994) 258–262.
- [17] J. Donohue, *The Structure of the Elements*. Wiley, New York, 1974.
- [18] R.W.G. Wyckoff, *Crystal Structures*, second ed. Interscience, New York, 1963.
- [19] V.V. Lemanov, *Phys. Solid State* 39 (1997) 1468–1473.
- [20] O. Madelung, M. Schulz, H. Weiss, *Numerical Data and Functional Relationships in Science and Technology*, vol. 17, Springer-Verlag, Berlin, 1982.
- [21] S.A. Pianaro, P.R. Bueno, P. Olivi, E. Longo, J.A. Varela, *J. Mater. Sci. Mater. Electron.* 9 (1998) 159–165.
- [22] O.L. Anderson, P. Andreatch, *J. Am. Ceram. Soc.* 49 (1966) 404–409.
- [23] J.D. Jorgensen, *J. Appl. Phys.* 49 (1978) 5473.
- [24] R.E. Newnham, Y.M. de Haan, *Z. Krist.* 117 (1962) 235–237.
- [25] A. Alkauskas, P. Broqvist, A. Pasquarello, *Phys. Rev. Lett.* 101 (2008) 046405.